Moroccan Journal of Chemistry
ISSN : 2351-812X

Mor. J. Chem., 2023, Volume 11, Issue 4, Page 1027-1037
https://revues.imist.ma/index.php/morjchem
https://doi.org/10.48317/IMIST.PRSM/morjchem-v11i04.41242

Electrochemical Impedance Spectroscopy Investigation of Self-Healing Coatings Based on Epoxy/Resole (IPNs) Incorporated with ppy@nano(SiO_2/ZnO/Fe_3O_4)

Dalal A. Mohammed [1, *], Salah S. Al-Luaibi [1, **], Hadi Al-Sawaad[1,*]**
[1] Department of Chemistry, science collage, University of Basra, IRAQ.
**Corresponding author, Email address: daloalaana58@gmail.com*
***Corresponding author, Email address: salah.hashim@uobasrah.edu.iq*
****Corresponding author, Email address: hadi.ziara@uobasrah.edu.iq*

Received *30 June 2023,*
Revised *29 July 2023,*
Accepted *01 Aug 2023*

Citation*: Mohammed D. A., Al-Luaibi S. S., Al-Sawaad H. (2023) Electrochemical Impedance Spectroscopy Investigation of Self-Healing Coatings Based on Epoxy/Resole (IPNs) Incorporated with ppy@nano (SiO_2/ZnO/Fe_3O_4), Mor. J. Chem., 11(4), 1027-1037*

Abstract: This study employed core-shell polymerization to synthesize three types of interpenetrating polymer networks (IPNs): (epoxy / resole) IPN/ppy@nanoSiO_2, (Epoxy /resole) IPN/ppy@nanoZnO, and (epoxy - resole) IPN/ppy@nanoFe_3O_4. The prepared compounds were subjected to comprehensive characterization using Fourier Transform Infrared Spectroscopy (FTIR), Scanning Electron Microscopy (SEM), Transmission Electron Microscopy (TEM), X-Ray Diffraction (XRD), Thermogravimetric Analysis (TGA), and Differential Scanning Calorimetry (DSC) techniques. These IPNs were subsequently applied as self-healing coatings on carbon steel (C1010) alloy. The inhibition efficiencies of the coated carbon steel were then evaluated in a 1M HCl solution using Electrochemical Impedance Spectroscopy (EIS). The results demonstrated an increase in the Rp values according to the following order: (epoxy /resole) IPN/ppy@nanoSiO_2 > (epoxy / resole) IPN/ppy@nanoZnO > (epoxy/ resole) IPN/ppy@nanoFe_3O_4. Notably, the (epoxy /resole) IPN/ppy@nanoSiO_2 coating exhibited a remarkable inhibition efficiency of 100%.

Keywords: *ppy@nano(SiO2/ZnO/Fe3O4), IPNs, EIS, Corrosion, Coating*

1. Introduction

In recent years, the development of self-healing coatings has garnered considerable attention as a promising technology that offers autonomous damage repair and surface protection. These coatings incorporate functional agents within their matrix, enabling them to respond to external stimuli such as heat, light, or mechanical force, and initiate the healing process. Numerous research efforts have been dedicated to advancing self-healing coatings across various industries including aerospace, automotive, and marine sectors (Wang *et al*. 2014; Karekar *et al*. 2018; Neto *et al*. 2020; Mohamed *et. al.* 2022; Andreia *et al*. 2021; Piao *et al*. 2022; Soliman *et al*. 2023). Within the realm of corrosion protection, significant progress has been made in the synthesis and characterization of self-healing coatings utilizing poly pyrrole (PPy) and metal oxide nanoparticles. PPy, a conductive polymer possessing

inherent self-healing properties, has demonstrated potential as an effective corrosion inhibitor. Extensive studies have focused on evaluating the self-healing capabilities of PPy coatings, showcasing their ability to mend cracks and defects resulting from corrosion, thereby enhancing overall corrosion resistance. Factors such as PPy concentration, pH, and applied potential have been explored to understand their influence on the self-healing behavior of PPy coatings (Paliwoda-Porebska *et. al.* 2005). Furthermore, metal oxide nanoparticles like zinc oxide (ZnO) and cerium oxide (CeO_2) have been investigated as alternative self-healing corrosion inhibitors (Ziouche *et.al.* 2021). These nanoparticles exhibit the capacity to release corrosion inhibitors in response to environmental changes, such as variations in pH or the presence of corrosive substances. Research has demonstrated that the integration of metal oxide nanoparticles into coatings significantly improves the corrosion resistance of metal surfaces. Moreover, their self-healing properties enhance their performance under harsh conditions. (Michele Fedel *et. al.* 2013; Jian *et. al.* 2020; Yin *et al.* 2020; Jadhav *et. al.* 2010; Guo *et.al.* 2022)

In recent years, hybrid coatings combining PPy and metal oxide nanoparticles have gained increased attention. These hybrid coatings exhibit enhanced self-healing capabilities and improved corrosion protection compared to individual coatings. Ongoing research focuses on optimizing the composition and structure of these hybrid coatings to achieve optimal performance in terms of self-healing ability and corrosion resistance. (Shuo Tang, *et. al.* 2023; Mousa *et. al.* 2023; Dagdag *et. al.* (2017).

This paper presents the results of a comprehensive investigation into the corrosion resistance of hybrid coatings utilizing Electrochemical Impedance Spectroscopy (EIS) techniques. The study focuses on the utilization of Epoxy/Resole Interpenetrating Polymer Networks (IPNs) incorporated with ppy@nano(SiO_2/ZnO/Fe_3O_4) for this purpose.

2. Methodology

2.1 Sourcing and preparation of Polymers

All chemicals utilized in this experiment were procured from BDH. Prior to polymerization, pyrrole underwent a distillation process.

2.2 Instruments

Fourier-transform infrared spectroscopy analysis was performed using a Perkin ElmeSpectrum 100 FT-IR Spectrometer (PerkinElmer, Waltham, MA, USA), The thermal analyses (DTA/TGA) of the raw DE were carried out in air conditions using a Universal V4.5A TA Instrument, SDT Q600 V20.9 Build 20 apparatus, The surface morphology of the products was determined using FEI NOVA Nano SEM 450). Electrical impedance spectroscopy EIS measurements were preformed using model corr Test –CS350

2.3 Experiments

Synthesis polypyrrole

A solution of 25 mL deionized water and 8.5 mL of distilled pyrrole monomer were stirred for 10 minutes with a magnetic stirrer. A 2.5 M solution of FeCl3 was then slowly added to the mixture to initiate the polymerization reaction, resulting in the formation of black precipitates in the flask. The reaction was allowed to proceed for 24 hours at room temperature, and the precipitate was then filtered several times using filter paper to remove any residual oxidant or impurities. The resulting purified precipitate was dried in a vacuum oven at 60-80°C until a constant weight was achieved. Abdirahman Yussuf *et. al.* (2018)

Synthesis of (polypyrrole @ metal oxide) using core shell polymerization

In this experiment, core-shell polymerization was prepared by dispersing 2.8 mL of pyrrole monomer in 100 mL of deionized water and mixing it with 5.6g of SiO_2 nanoparticles using an ultrasonic water bath. A solution of 3 g SDS and 1 M $FeCl_3$ was mixed and then slowly added for in situ polymerization of PPy. The resulting product was filtered, washed, and dried to obtain a solid SiO_2/PPy nanocomposite. Similar procedures were used to prepare other nanocomposites of ppy/Fe_3O_4 and ppy/ZnO **(**Kwang-Hyok Han *et. al.* 2022)

Synthesis self-healing IPN Coating

The epoxy resin was dissolved in toluene and mixed with metal oxide polypyrrole in a 1:1 weight ratio. The mixture was sonicated for 30 minutes until uniformly spread, and then the amine hardener was added in a ratio of 1:0.5. The components were mixed and the epoxy resin was allowed to partially cure. Next, resole resin was added in a 1:1 weight ratio and the mixture was sonicated for an additional 30 minutes. Finally, the resulting interpenetrating polymer network (IPN) was used as a coating for carbon steel spacecraft and dried under 100°C for 5 hours.

2.3 Product characterisation

In the IR spectrum **Figure (1)** of polypyrrole, the broad and strong absorption peak around 3400 cm-1 is associated with the stretching vibration of the N-H bond in the pyrrole rings. The peak around 2900 cm^{-1} is due to the stretching vibration of C-H bonds in the aromatic ring. The peaks around 1570 cm^{-1} correspond to the stretching and bending vibrations of the C=C bond in the pyrrole ring. The peak at around 1300 cm-1 corresponds to the C-N stretching vibration of the pyrrole ring. The peak at around 1000 cm^{-1} is due to the C-H bending vibration in the aromatic ring. The broad peak around 600-800 cm^{-1} corresponds to the out-of-plane deformation of the pyrrole ring.

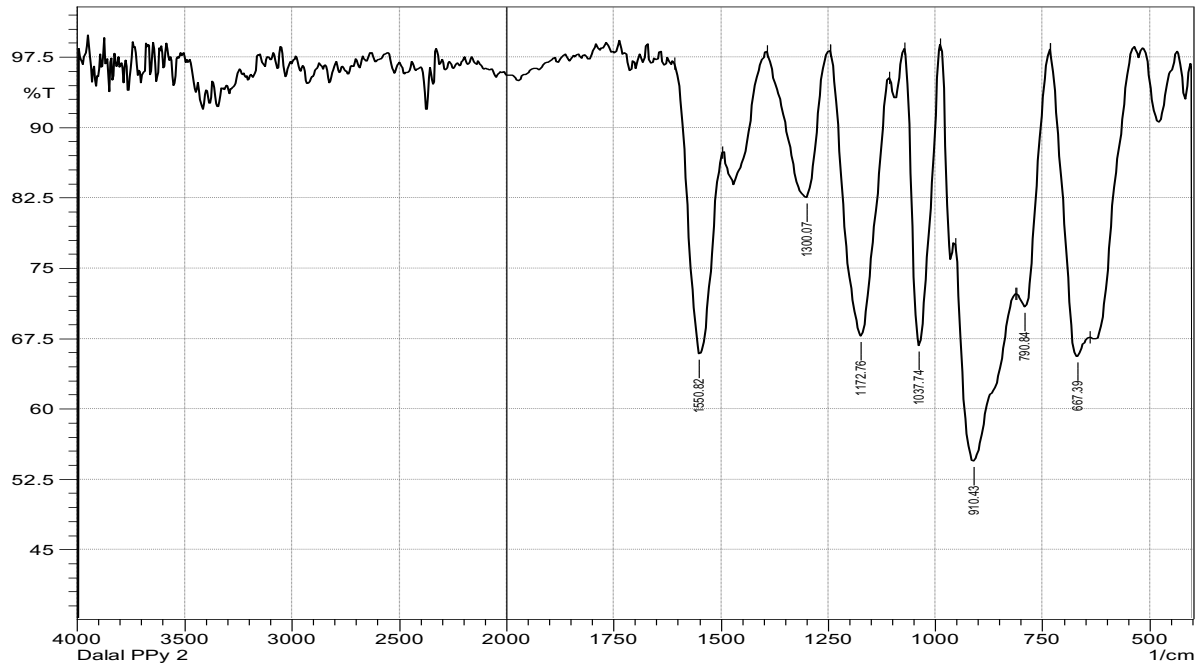

Figure 1. FTIR spectrum for PPY

Figure (2) showed that infrared spectrum of PPy-SiO_2 core shell polymerization the stretching vibrations of the Si-O bonds in SiO_2 typically produce absorption bands in the infrared region between

1000 and 1200 cm^{-1}, with a characteristic peak around 1100 cm^{-1}. The bending vibrations of the Si-O-Si bonds typically produce absorption bands in the region between 400 and 800 cm-1, with a characteristic peak around 460 cm^{-1} (Daliana Muller *et al*. 2015).

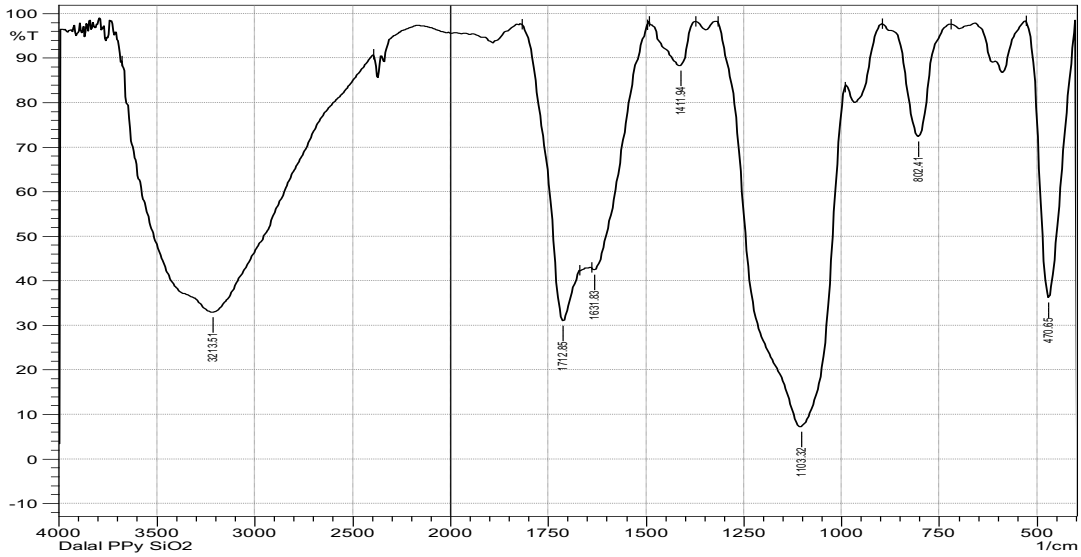

Figure 2. FTIR spectrum for PPY-SiO2

3-Results and discussion

3.1XRD

X-ray diffraction (XRD) of poly pyrrole **figure (3)** can provide information on its crystalline structure and morphology. Polypyrrole usually shows broad peaks in the XRD pattern due to its amorphous nature, although some weak peaks may also be observed corresponding to certain crystalline planes. The main peak in the XRD pattern is typically observed at around 2θ= 25-30°, which corresponds to the (100) plane of the polymer backbone. Additional peaks in the XRD pattern at 2θ values of 10-15° and 35-40° may also be present, corresponding to the (001) and (200) planes, respectively. These peaks can be indicative of a higher degree of crystallinity or orientation in the polymer. The XRD pattern can also provide information on the inter-chain spacing or distance between adjacent polymer chains, which can influence the conductivity and other properties of the material (Daliana Muller *et al.* 2015).

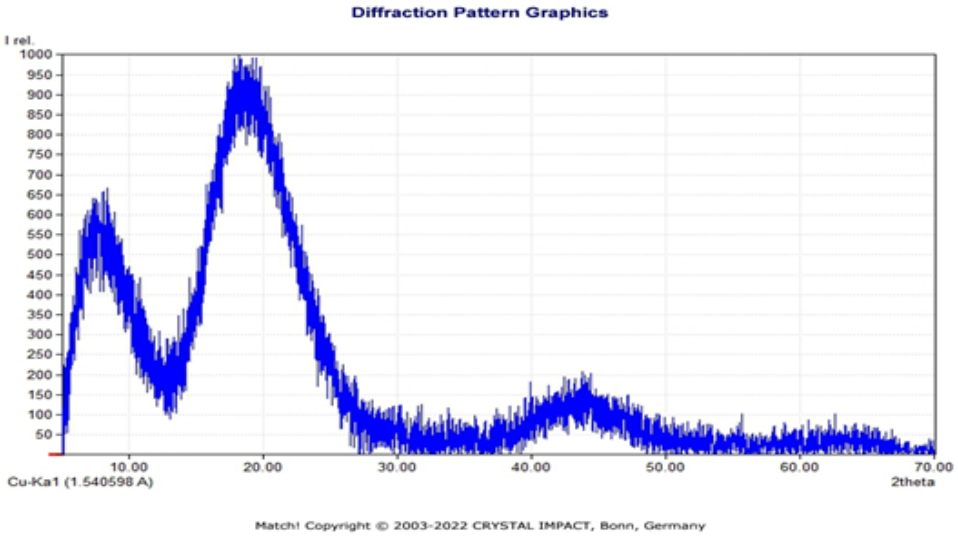

Figure (3) XRD of ppy

3.2TGA and DSC Thermograms

The combination of TGA and DSC **Figure (4)** can provide complementary information about the thermal behavior of polypyrrole. The TGA can provide information about the thermal stability and decomposition behavior of the polymer, (Nazarenko *et al.* 2016), while the DSC can provide information about its thermal transitions and other properties. The results from both techniques can be useful in optimizing the processing conditions and understanding the thermal behavior of IPNs for different applications. In the TGA of IPNs, the initial weight loss observed at lower temperatures is due to the evaporation of any residual solvent or water present in the sample. The subsequent weight loss that occurs at higher temperatures is due to the decomposition of the IPNs, which can provide information about its thermal stability. DSC measures the heat flow associated with a sample as a function of temperature. The DSC of IPNs can provide information about its glass transition temperature (Tg), melting point (Tm), and other thermal properties. The Tg of polypyrrole is usually observed as a step change in heat flow at a lower temperature, while the Tm, not observe (Ennis *et al.* 1993).

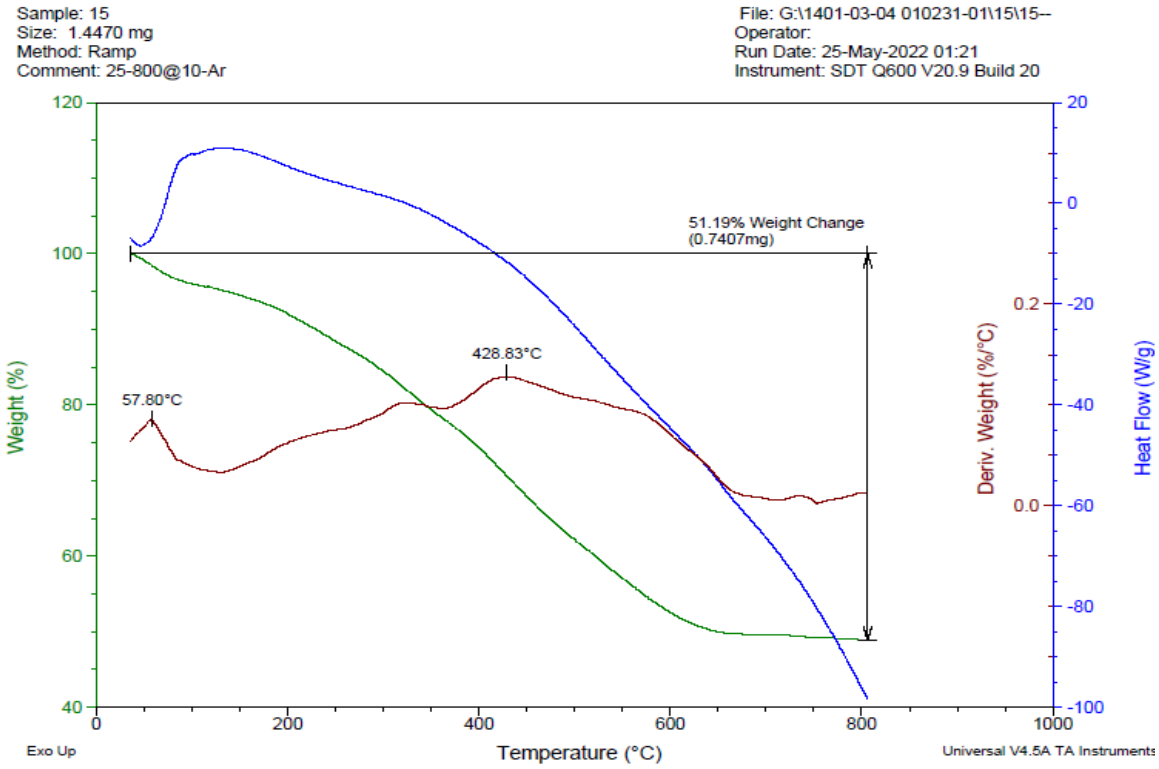

Figure (4) TGA and DSC for IPNs

3.3 Surface morphology

Interpretation of microscopy images **figs (5,6)** of polypyrrole (PPy) nano metal oxide (NMO)IPNs would involve analyzing the structure and morphology of the material at the nanoscale. SEM would provide information on the surface morphology and topography of the PPy NMO, while TEM would allow for the analysis of the internal structure and crystallography of the material. The specific interpretation would depend on the characteristics of the images, such as particle size, shape, and distribution, as well as the type of metal oxide used and the synthesis method employed (Daliana Muller *et al.* 2015)

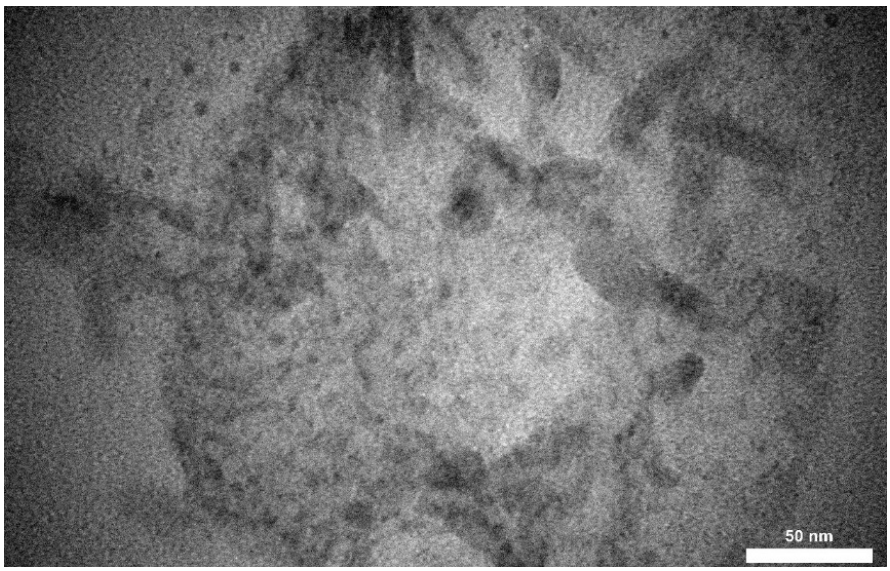

Figure 5. TEM micrograph of IPNs

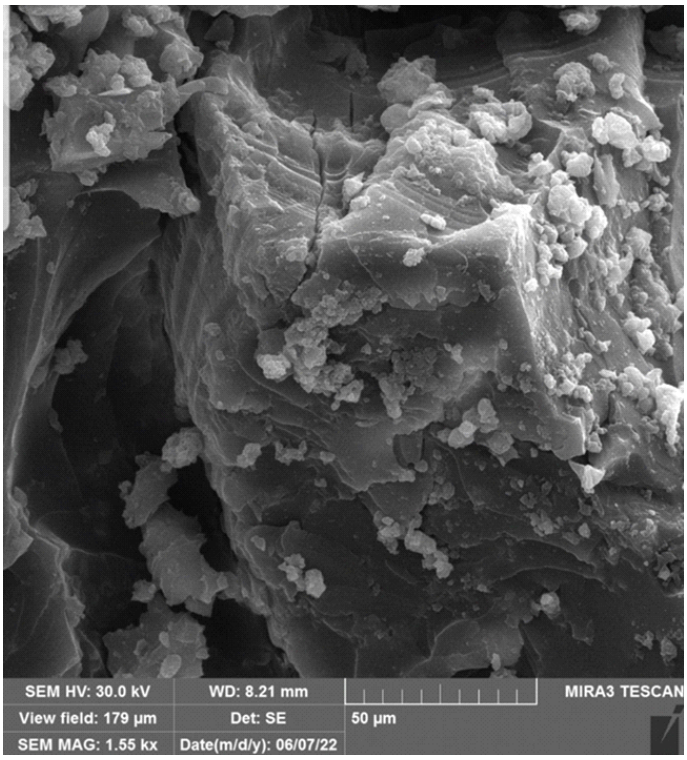

Figure 6 SEM for IPNs

3-4Electrical impedance spectroscopy EIS measurements

A Nyquist plot is a graphical representation of the impedance response of a material as a function of frequency **figure (7)** and **Table (1)** It is created by plotting the imaginary component of impedance (Z") versus the real component of impedance (Z') on a logarithmic scale. The plot is typically displayed in a semicircle or an arc in the high-frequency region, which is caused by the presence of a capacitive element. The straight line in the low-frequency region is caused by the resistive element. In the case of epoxy resin and resole, the Nyquist plot might show a semicircle in the high-frequency region due to the presence of a capacitive element, which would correspond to the dielectric properties of the material. The resistive element in the low-frequency region might correspond to the conductivity of the material. The position and size of the semicircle on the plot can provide information on the

capacitance, resistance, and dielectric constant of the material (Zhang *et al*. 2015; Eziuka *et al*. 2023; Chami *et al*. 2023). Bode plots **figure (7)** are instrumental in understanding the underlying mechanisms governing the electrochemical system, aiding in the development of more efficient and reliable electrochemical devices and materials.

In the case of PPy @ nano SiO2, the Nyquist plot might show a depressed semicircle in the high-frequency region due to the capacitive effect of the nanoparticles. The size and shape of the semicircle would provide information on the dielectric properties of the nanocomposite. The presence of of PPy @ nano SiO2 could also affect the interfacial resistance between the epoxy resin and the resole, which would be reflected in the position of the semicircle on the plot. The polarization resistance (Rp) is a measure of the resistance to charge transfer at the interface between the coating and the electrolyte solution. It is typically measured by electrochemical impedance spectroscopy (EIS) and can be used to evaluate the corrosion resistance of a coating. It was found to have 100% efficiency.as the following order:

(Epoxy/resole)IPN/ppy@nanoSiO2>(Epoxy/resole)IPN/ppy@nanoZnO>
(Epoxy/resole)IPN/ppy@nanoFe3O4

The order of the Rp values might be due to the differences in the morphology, composition, and interfacial properties of the coatings. A higher Rp value indicates better corrosion resistance. (Epoxy/resole)IPN/ppy@nanoSiO_2 coatings might have a higher Rp value than (Epoxy/resole)IPN/ppy@nanoZnOand(Epoxy/resole)IPN/ppy@nanoFe_3O_4 coatings because of the unique properties of SiO2, such as its high dielectric constant and low ionic conductivity.

Table (1) : Some corrosion parameters from EIS

Polymeric coating	Rp(Ω.cm2)	Fmax (Hz)	Cdl(µf.cm-2)	τ*103 (s)	%IE
Blank	11.15	939.13	1.52069E-05	0.000169557	-
Epoxy	14.5	232.3	4.72741E-05	0.000685474	23.10344828
Resole	32.71	7854.6	6.19777E-07	2.02729E-05	65.91256496
(Epoxy/Resole) IPNs	24655	15709	4.11137E-10	1.01366E-05	99.95477591
(Epoxy/Resole) IPNs/ppy	4.56E+04	469.57	7.43775E-09	3.39E-04	1.00E+02
(Epoxy/Resole)IPNs/ppy@NanoSiO_2	1.56E+07	114.3	8.92008E-11	1.39E-03	1.00E+02
(Epoxy/Resole)IPNs/ppy@NanoZnO	2.87E+05	56.8	9.7664E-09	2.80E-03	1.00E+02
(Epoxy/Resole)IPNs/ppy@NanoFe_3O_4	7.92E+04	28.3	7.10559E-08	5.63E-03	1.00E+00

The addition of PPy to SiO_2 might enhance the electrical conductivity of the coating, leading to a higher Rp value. (Epoxy+resole)IPN/ppy@nanoZnO coatings might have an intermediate Rp value because ZnO is a good corrosion inhibitor and PPy can enhance the electrical conductivity of the coating. The presence of ZnO nanoparticles could increase the interfacial resistance, resulting in a lower Rp value than (Epoxy+resole)IPN/ppy@nanoZnO coatings. (Epoxy+resole)IPN/ ppy@nanoFe_3O_4 coatings might have the lowest Rp value due to the lower corrosion inhibition properties of Fe_3O_4 and the possible formation of a passive layer at the coating/electrolyte interface, which could reduce the Rp value. Han *et al.* 2022 postulated that the PPy layer caused the decrease in intensity of three previous parts and the increase in the crystal size of nanocomposites. high amount of Fe_3O_4 nanoparticles in PPy may be required for applications like flame retardant coatings (Jouyandeh *et al.* 2019). Furthermore, the addition of Gold to PPY@Fe3O4 nanocomposites improves a highly versatile multifunctional

leading to great potential in simultaneous multimodal imaging-guided cancer theranostic applications (Feng *et al.* 2015).

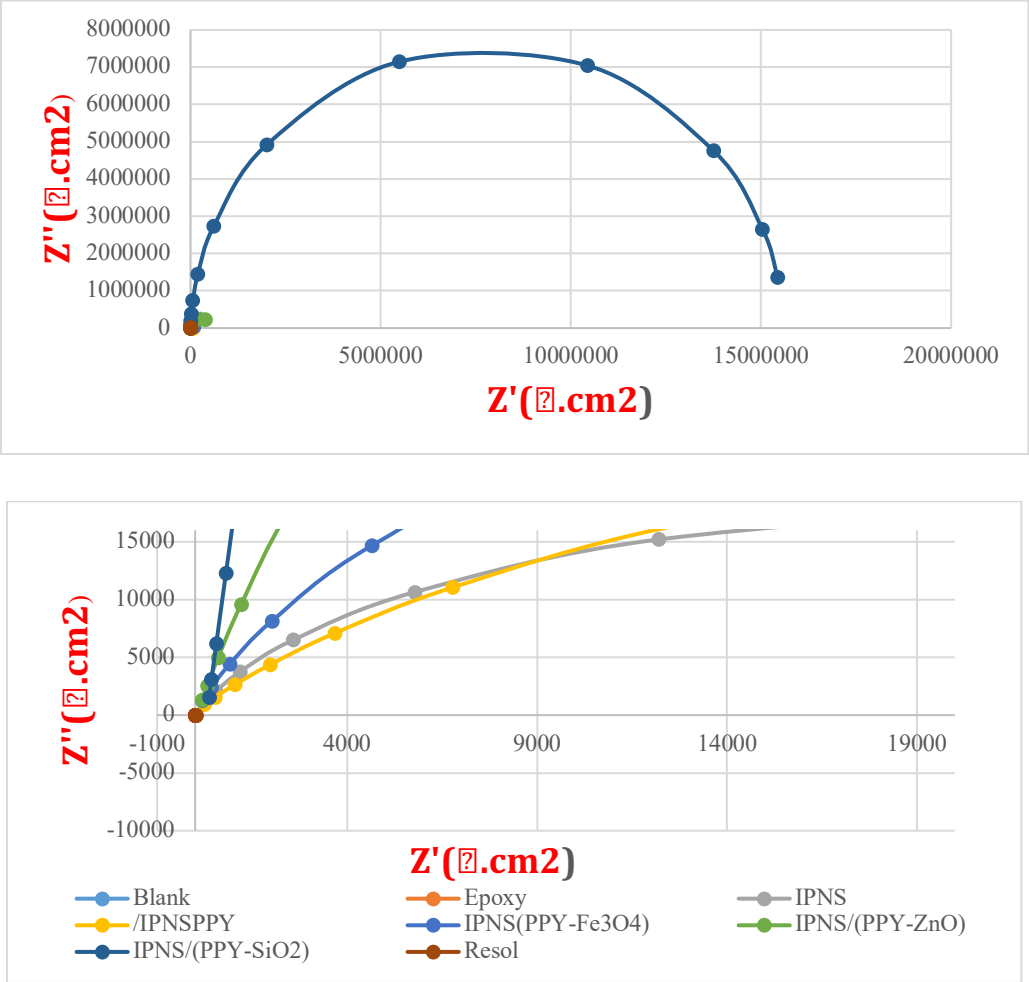

Figure 7. Nyquist plote, 1 M HCl at 298K

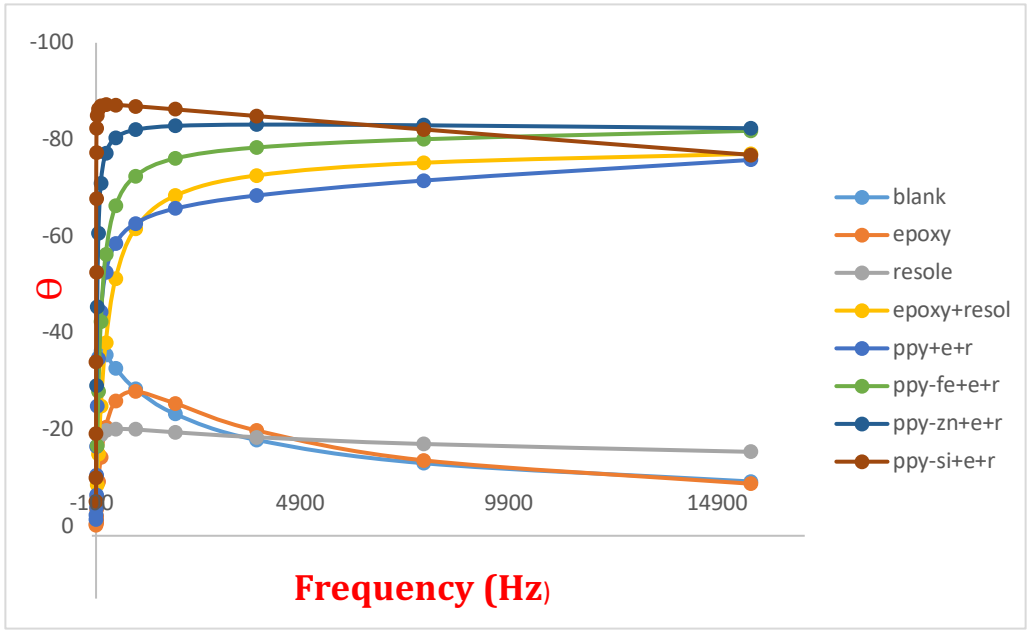

Figure 8. Bode plot, 1 M HCl at 298K

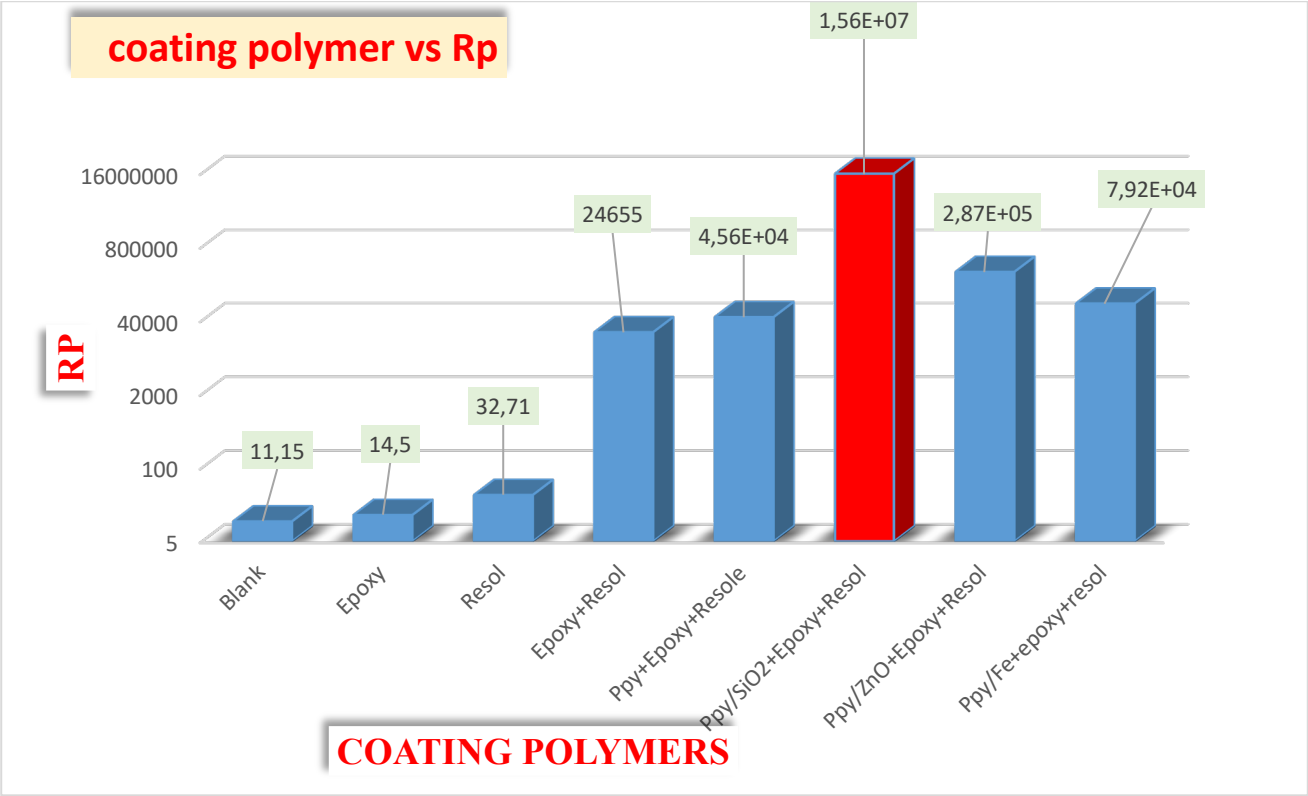

Figure 9. relationship of Rp vs Polymers coating

Conclusion

In conclusion, this study investigated the synthesis and characterization of self-healing coatings based on epoxy/resole interpenetrating polymer networks (IPNs) incorporated with ppy@nano(SiO_2/ZnO/Fe_3O_4). The prepared IPNs were extensively characterized using various techniques such as FTIR, SEM, TEM, XRD, TGA, and DSC. The coatings were applied on carbon steel alloy and their inhibition efficiencies were evaluated using electrochemical impedance spectroscopy (EIS) in a corrosive environment. The results showed that the (epoxy/resole) IPN/ppy@nanoSiO_2 coating exhibited the highest inhibition efficiency of 100%. This study demonstrates the potential of these self-healing coatings for corrosion protection in various industries. Further optimization of the composition and structure of these coatings can lead to even better performance in terms of self-healing ability and corrosion resistance.

Disclosure statement: *Conflict of Interest:* The authors declare that there are no conflicts of interest.
Compliance with Ethical Standards: This article does not contain any studies involving human or animal subjects.

References

Abdirahman Y., Mohammad A., Salah Al., & Gils A. (2018), Synthesis and Characterization of Conductive Polypyrrole: The Influence of the Oxidants and Monomer on the Electrical, Thermal, and Morphological Properties, *International Journal of Polymer Science,* ID 4191747, https://doi.org/10.1155/2018/4191747

Andreia A. F., Francisco J. G., Arnaldo G. P., & Vitor F. C. Sousa. (2021), Characterization of Thin Chromium Coatings Produced by PVD Sputtering for Optical Applications, *Coatings,* 11(2), 215; https://doi.org/10.3390/coatings11020215

Dagdag O., El Gouri1 M., Ebn Touhami M., & El Harfi A. (2017), Evaluation of corrosion protection of epoxy coatings on copper during exposure to an aerated 3% NaCl solution, *Mor. J. Chem.* 5 N°1, 120-130.

Daliana M., Geneviève K. P., Tatiana B., Alberto J. G., (2015), Synthesis of Conductive PPy/SiO_2 Aerogels Nanocomposites by In Situ Polymerization of Pyrrole, *Journal of Nanomaterials,* 658476, doi.org/10.1155/2015/658476

Chami A., Benabbou R., Taleb M. 2, Rais Z., El Haji M, (2023), Inhibition of corrosion of steel in 1 M HCl solution by polyphenol extract: Application for Steel used in the automotive industry in Morocco, *Mor. J. Chem.,* 14(3), 623-644, https://doi.org/10.48317/IMIST.PRSM/morjchem-v11i3.37787

Ennis B.C. & Truong V.-T., (1993), Thermal and electrical stability of polypyrrole at elevated temperatures, *Synthetic Metals,* 59, 3, 387-399, https://doi.org/10.1016/0379-6779(93)91170-7

Eziuka J. E., Onyeachu I.B., Njoku D.I., Nwanonenyi S.C., Chidiebere M. A., Oguzie E. E., Eziuka et al. (2023), Elucidating the inhibition behavior of Pterocarpussantalinoides leaves extract on mild steel corrosion in H_2SO_4 solution–GC-MS, FTIR, SEM, Experimental and computational approach, *Mor. J. Chem.,* 14(3), pp. 579-593, https://doi.org/10.48317/IMIST.PRSM/morjchem-v11i03.39198

Fedel M., Ecco L. G., Ahniyaz A., & Deflorian A. (2013), Influence of polyaniline and cerium oxide nanoparticles on the corrosion protection properties of alkyd coating, *Progress in Organic Coatings*, DOI:10.1016/j.porgcoat.2014.04.002

Feng W.; Zhou X.; Nie W.; Chen L.; Qiu K.; Zhang Y.; He C. (2015) Au/polypyrrole@ Fe3O4 nanocomposites for MR/CT dual-modal imaging guided-photothermal therapy: An in vitro study. *ACS Appl. Mater. Interfaces*, 7, 4354–4367.

Guo, L.; Wang, H.; Li, X.; Fei, G.; Yuan, Y.; Li, Y. (2022) A Synergistic System of Polyaniline@ Graphene-Alkyd Resin via Gemini Surfactant for Enhanced Anti-Corrosion Properties. *Prog. Org. Coat.,* 170, 106944, DOI: 10.1016/j.porgcoat.2022.106944

Han K.H., Kim Y.H., Mun M.H., Yu J.H., & Han R.H. (2022), Synthesis of polypyrrole-modified $Fe_3O_4/SiO_2/TiO_2$ nanocomposite microspheres and their photocatalytic activity, *Materials Research Express,* 9(2), 025007, DOI 10.1088/2053-1591/ac5195

Heimann RB. (2020) Magnesium alloys for biomedical application: advanced corrosion control through surface coating. *Surf Coatings Technol*.; 405, 126521. https://doi.org/10.1016/j.surfcoat.2020.126521

Jadhav R.S.; Hundiwale D.G.; Mahulikar P.P. (2010) Synthesis of Nano Polyaniline and Poly-o-Anisidine and Applications in Alkyd Paint Formulation to Enhance the Corrosion Resistivity of Mild Steel. *J. Coat. Technol. Res, 7*, 449–454, doi:10.1007/s11998-009-9214-0.

Jian SY, Yang C. Y., & Chang J. K. (2020), Corrosion resistance and self-healing characteristics of a novel Ce/Mn conversion coatings on EV31 magnesium alloys. *Appl Surf. Sci.* 510, 145385 https://doi.org/10.1016/j.apsusc.2020.145385

Jouyandeh M., Rahmati N., Movahedifar E., Hadavand B. S., Karami Z., Ghaffari M., Taheri P., Bakhshandeh E., Vahabi H., Ganjali M. R., Formela K., Saeb M. R. (2019) Properties of nano-Fe3O4 incorporated epoxy coatings from Cure Index perspective, *Progress in Organic Coatings,* 133, 220-228, ISSN 0300-9440, https://doi.org/10.1016/j.porgcoat.2019.04.034

Karekar S.E.; Bagale U.D.; Sonawane S.H.; Bhanvase B.A.; Pinjari D.V. (2018) A Smart Coating Established with Encapsulation of Zinc Molybdate Centred Nanocontainer for Active Corrosion Protection of Mild Steel: Release Kinetics of Corrosion Inhibitor. *Compos. Interfaces,* 25, 785–808. https://doi.org/10.1080/09276440.2018.1439631

Mohamed N. S., Alias J., Johari N. A., Alang N. A., & Ahmad A. H. (2022), Development of smart self-healing coating for the corrosion protection of magnesium alloys: a brief review, *Journal of Adhesion Science and Technology,* https://doi.org/10.1080/01694243.2022.2158774

Mousa O.I., Al-Luaibi S.S., Al-Mubarak A.S., Lgaz H, Hammouti B., Chaouiki A., and Ko Y.G. (2023), On the Development of an Intelligent Poly(aniline-co-o-toluidine)/Fe3O4/Alkyd Coating for Corrosion Protection in Carbon Steel, *Appl. Sci,* 13, 8189 Doi.org/10.3390/app13148189

Nazarenko O.B., Melnikova T.V. & Visakh P.M. (2016), Thermal and Mechanical Characteristics of Polymer Composites Based on Epoxy Resin, Aluminium Nanopowders and Boric Acid, *Journal of Physics: Conference Series,* 671, 012040, doi:10.1088/1742-6596/671/1/012040

Neto A.G.C.; Pellanda A.C.; de Carvalho Jorge A.R.; Floriano J.B.; Berton M.A.C. (2020) Preparation and Evaluation of Corrosion Resistance of a Self-Healing Alkyd Coating Based on Microcapsules Containing Tung Oil. *Prog. Org. Coat.*, 147, 105874. DOI:10.1016/j.porgcoat.2020.105874

Paliwoda-Porebska G., Stratmann M., Rohwerder M., Potje-Kamloth K., Lu Y., Pich A. Z. & Adler H. J. (2005), On the development of polypyrrole coatings with self-healing properties for iron corrosion protection, *Corrosion Science*, 47(12), 3216-3233, https://doi.org/10.1016/j.corsci.2005.05.057

Piao J.; Wang W.; Cao L.; Qin, X.; Wang T.; Chen S. (2022) Self-Healing Performance and Long-Term Corrosive Resistance of 386 Polyvinylidene Fluoride Nanofiber Alkyd Coating. *Compos. Commun.,* 36, 101404. DOI: 10.1016/j.coco.2022.101404

Soliman H.A., Ibrahim M.M., Ali L.I., Saif M., Abdelshafi N.S. & Khaled K.F., (2023) Nano-Yttrium Titanate Coated 304 Stainless Steel: Preparation, Characterization, and Corrosion Protection Application, *Mor. J. Chem.,* 11, 3, 780-801, Doi.org/10.48317/IMIST.PRSM/morjchem-v11i3.40959

Tang S., Lei B., Eng. Z., Guo H., Zhang P. & Meng G. (2023), Progress in the Graphene Oxide-Based Composite Coatings for Anticorrosion of Metal Materials, *Coatings,* 13(6), 1120; https://doi.org/10.3390/coatings13061120

Wang W.; Xu L.; Li X.; Lin Z.; Yang Y.; An E. (2014) Self-Healing Mechanisms of Water Triggered Smart Coating in Seawater. *J. Mater. Chem.* A, 2, 1914–1921. DOI:10.1039/C3TA13389C

Yin Z-Z., Qi W. C., Zeng R. C., Chen X. B., Gu C. D., Guan C. K., & Zheng Y-F. (2020). Advances in coatings on biodegradable magnesium alloys. *J Magnesium Alloys.;* 8(1), 42–65. https://doi.org/10.1016/j.jma.2019.09.008

Zhang Y.; Shao Y.; Meng G.; Zhang T.; Li P.; Wang F. (2015) Evaluation of the Corrosion Protection of Defective Polyaniline/Epoxy Coating by Localized Electrochemical Impedance Spectroscopy. *J. Coat. Technol. Res.,* 12, 777–785. DOI:10.1007/s11998-015-9679-y

Ziouche A., Hammouda A., Boucherou N., Mokhtari M., Hafez B., Elmsellem H., Abaidia S. (2021) Corrosion protection enhancement on aluminum alloy and magnesium alloy by Mo-CeO_2 conversion coating, *Mor. J. Chem.* 9(3), 386-393, https://doi.org/10.48317/IMIST.PRSM/morjchem-v9i3.27828